[18F]Sodium-Fluoride PET/MRI Monitoring of Hormonal Therapy Response in Breast Cancer Bone Metastases–Proof of Concept

Maira Zia[1*], Elin Lundström[1], Johanna Mårtensson[1], Mark Lubberink[1, 2], Aglaia Schiza[3, 4] and Anders Sundin[1]

[1]Department of Surgical Sciences, Radiology, Uppsala University Hospital, Akademiska sjukhuset, Uppsala, Sweden

[2]Medical Physics, Uppsala University Hospital, Akademiska sjukhuset, Uppsala, Sweden

[3]Department of Immunology, Genetics and Pathology, Science of Life Laboratory, Uppsala University, Uppsala, Sweden

[4]Department of Oncology, Uppsala University Hospital, Akademiska sjukhuset, Uppsala, Sweden

Abstract

RECIST 1.1 tumour size measurements on CT/MRI are the mainstay of cancer therapy monitoring. However, bone metastases are consistently difficult to evaluate for hormonal therapy response often escaping CT detection. This study aimed to assess dynamic and static [18F]sodium fluoride-([18F]NaF)-PET/MRI by combining standardized uptake value (SUV) and net influx rate (K_i) from PET with the apparent diffusion coefficient (ADC), proton density fat fraction (PDFF) and effective transverse relaxation rate (R_2^*) from MRI for monitoring hormonal therapy effect on bone metastases. In this prospective study, three breast cancer patients underwent a 60-minute dynamic whole-body [18F]NaF-PET/MRI before and after hormonal therapy. In PET images, pelvic and spine metastases (approx. n=10/patient) with high/intermediate uptake were delineated by applying an adaptive threshold algorithm to provide SUV_{mean} and SUV_{max}. Pharmacokinetic modeling was performed and K_i was calculated using a two-tissue reversible model. VOI measurements of ADC, PDFF and R_2^* utilized the OLEA medical software. The changes between baseline and follow-up data were calculated, statistically analysed and utilized linear regression. [18F]NaF-PET/MRI provided a powerful method for monitoring hormonal therapy response in breast cancer bone metastases as reflected by decreases in SUV and K_i. MRI parameters showed changes consistent with therapy response, although only R_2^* reached statistical significance.

Keywords: Breast cancer • Bone metastases • 18F-fluoride • K_i • PET/MRI • ADC • PDFF • R_2^* • Therapy response monitoring • PET/CT

Introduction

Breast cancer is the most commonly diagnosed cancer in women and yet remains the leading cause of cancer-related deaths in women worldwide. Breast cancer most commonly metastasize to bone, being the only metastatic site in 28%-44% of the metastatic breast cancer (MBC) patients [1]. Bone-only metastasis is followed in frequency by multiple metastasis, mainly to lung, pleura, liver and brain. The disease is more stable in patients who first develop skeletal metastases than visceral metastases [2]. Bone metastases may during a prolonged clinical course be responsible for much of the morbidity in breast cancer patients, many of whom at some point encounter skeletal-related events. The first-line treatment for metastatic hormone receptor-positive breast cancer and in particularly for patients with only bone metastases is hormonal therapy in combination with bone-modifying agents [3].

Various imaging modalities have been used to assess bone metastasis for treatment response in MBC. When responding to hormonal therapy, lytic metastases typically show osteosclerosis within the bone marrow in the form of micro-calcification, generally escaping detection on both plain film X-ray and computed tomography (CT). CT frequently fails to visualize bone metastasis, and therefore magnetic resonance imaging (MRI) is increasingly employed, showing high sensitivity (95%) and specificity (90%) [4]. MRI is excellent for assessing metastatic spread to the bone marrow cavity, but for monitoring of therapy response, the conventional morphological MRI sequences need to be combined with diffusion-weighted imaging (DWI)

to assess the bone marrow cellular density. Because malignant tumours generally are hypercellular with a high nuclear/cytoplasmic ratio, and hence reduced molecular diffusion space is in all dimensions, quantification of the apparent diffusion coefficient (ADC) from DWI provides a means to assess the cellular density by measuring the water diffusion, shown feasible in previous studies [5]. According to RECIST 1.1, bone metastases are not measurable and thus only accounted for as non-target lesions [6]. Although CT may detect a lytic bone metastasis when becoming sclerotic, visualization of micro-calcifications, as an early sign of favourable therapy response, remains difficult to detect. Because of the high sensitivity and specificity of [18F] sodium fluoride ([18F]-NaF) positron emission tomography (PET)/CT for detection of bone metastasis, 100% and 97%, respectively [4], and the means for quantitative measurements provided by PET, the combination of [18F]NaF-PET and MRI (PET/MRI) may therefore prove effective, not only for visualization, but also for assessing changes in bone metastases in response to anticancer therapy.

Previous 18F-NaF-PET/CT studies have investigated the precision and suitability of PET quantification, concentrating on the standardized uptake value (SUV), and functional volume and of the transport rate constants and net influx, on static and dynamic PET, respectively [7]. And in one report also on therapy monitoring of MBC [8]. In dedicated MRI studies, DWI has been investigated for therapy monitoring of bone metastases [9]. However, to the best of our knowledge, hybrid imaging by [18F] NaF PET/MRI to assess anticancer therapy and specifically hormonal therapy response in skeletal MBC has not previously been applied. In the present study,

hormonal therapy response was therefore assessed in terms of changes in bone remodeling on [^{18}F]NaF PET/MRI by quantifying the net influx rate (K_i), SUV_{mean}, SUV_{max}, proton density fat fraction (PDFF), effective transverse relaxation rate (R_2^*) and DWI-derived ADC. The PET and MRI parameters were compared and correlated to the clinical response of the patients.

Materials and Methods

Patients

This prospective study included three female patients (aged 65, 75 and 80 years) recruited from the Department of Oncology at Uppsala University Hospital. All patients had MBC and bone metastasis in the spine and pelvis, and were treatment naïve for MBC. The patients underwent two PET/MRI examinations, once at baseline prior to therapy and once 3-6 months after therapy. After the baseline PET/MRI examination, treatment was administered according to standard-of-care by the oncologist: Letrozole n=2, Tamoxifen n=1 and all three were receiving the Receptor Activator of Nuclear factor Kappa-B Ligand (RANK-L) antibody, denosumab.

Ethical considerations

The study was approved by the Swedish Ethical Review Authority (no. 2016/492) and was conducted according to the principles expressed in the 1964 Declaration of Helsinki and its later amendments and comparable ethical standards.

PET acquisition and reconstruction

PET/MRI was commenced simultaneously with intravenous injection of [^{18}F]NaF (3 MBq/kg). Dynamic PET of the pelvis and the lower lumbar spine was acquired in list-mode with continuous registration for 60 minutes and reconstructed into 24 time-frames (10 × 30, 5 × 60, 5 × 120, 4 × 600 s). After this, a whole-body PET scan was acquired from the base of the skull to the proximal thighs (scan duration: 4 min/bed position). PET image reconstruction utilized Ordered Subset Expectation Maximization (OSEM). Images were reconstructed using time-of-flight ordered subset expectation maximization with 2 iterations and 28 subsets, including resolution recovery and a 5 mm Gaussian post-filter. Attenuation correction was based on a two-point Dixon sequence.

PET volumes of interest

The examinations were evaluated using the CARESTREAM Vue Picture Archiving and Communication System (PACS) software (Philips). Metastases were manually delineated on the whole-body [^{18}F]NaF-PET/MRI, both at baseline and 3-6 months after hormonal therapy start. Regions Of Interest (ROIs) were drawn by using a semi-automatically adaptive 50% cut-off threshold algorithm, occasionally followed by manual correction if deemed necessary. For each lesion, the two-dimensional ROIs were combined into a three-dimensional Volume Of Interest (VOI), for which SUV_{max} and SUV_{mean} were registered.

PET kinetic modeling

The last two frames of the dynamic scan (i.e., 40-60 min after injection) were summed to create an average image volume for visualising the anatomical orientation and facilitating a correct positioning of the ROIs. VOIs were drawn as described above. The plasma arterial input function was derived by measuring ^{18}F-fluoride counts over the descending aorta. Tissue time-activity curves were generated by projecting these VOIs on all individual time frames of the dynamic image sequence. Different kinetic models were assessed and a two-tissue reversible compartment model provided the best fit for our data.

Time-activity curves were analysed using a two-tissue reversible compartment analysis giving the rate constants K_1, k_2, k_3 and k_4 and the net influx rate K_i.

MRI data acquisition and reconstruction

The MRI protocol comprised the following sequences: Two-point Dixon sequence for attenuation correction (MR attenuation correction, MRAC, GE Healthcare), six-point Dixon for PDFF and R_2^* quantification (IDEAL-IQ, GE Healthcare), STIR for guidance in the delineation of the MRI data, and DWI with b-values; 50, 400, and 800 s/mm^2 for ADC assessment.

ADC, PDFF and R_2^* VOI measurements

ADC maps were derived from DWI data of b-value 50-800 s/mm^2, using the OLEA (Olea Medical, La Ciotat, France) medical software. Quantitative assessment of mean and median ADC, PDFF and R_2^* were obtained from VOIs manually delineated with OLEA. VOIs were drawn carefully to exclude the borders and the cortical bone in order to avoid partial volume effects. After validating VOIs on T1-weighted images, the VOIs were projected to ADC, PDFF and R_2^* data respectively and measurements were then registered.

Statistical methods

Statistical evaluation of the changes between baseline and follow-up examination was performed using Wilcoxon signed-rank test and regression analysis. Changes were presented as mean change and percentage change. P ≤ 0.05 was considered statistically significant.

Results

In the data analysis, an outlier lesion was found for SUV_{mean} and SUV_{max} and this metastasis was therefore excluded from all analyses.

K_i, SUV_{mean} and SUV_{max}

In each patient 5-7 pelvic and 3-4 spinal bone metastases with SUV_{max} ≥ 10 were chosen based on the highest [^{18}F]NaF uptake. The [^{18}F]NaF uptake in the spinal and pelvic bone metastases decreased from PET/MRI at baseline to follow-up: median K_i -41%, median SUV_{mean} -30% and median SUV_{max} -31%. K_i, SUV_{mean} and SUV_{max} in the pelvic metastases at baseline and at follow-up, their P values, and the respective changes are shown in Table 1 and Figure 1.

SUV_{mean} and SUV_{max} decreased or remained stable in all the lesions in patients with clinical non-progressive disease (non-PD). The relative decrease in SUV_{mean} and SUV_{max} was statistically significant, P=0.001 and P=0.004 respectively.

Regression analysis showed significant correlations between on one hand absolute changes in K_i and on the other hand SUV_{mean} and SUV_{max}, as shown in Figure 2 (R_2=0.706, P=0.0001 and R_2=0.685, P=0.00002, respectively).

ADC

In the patient-based analysis, the mean percentage change in ADC increased, ranging from 1% to 23%, which indicated therapy response. The baseline median ADC of the 17 pelvic lesions was 1158 × 10^{-6} mm^2/s and the follow-up median ADC was 1276 × 10^{-6} mm^2/s.

The median change in ADC at follow-up was 80 × 10^{-6} mm^2/s (5.1% increase) consistent with tumour necrosis, but not reaching statistical significance (P=0.081). The mean change in ADC ranged from 590 × 10^{-6} mm^2/s to -384 × 10^{-6} mm^2/s.

In a lesion-based analysis, 11/17 metastases at follow-up showed an increase in ADC. In 6/17 metastases, ADC decreased even though SUV_{mean}, SUV_{max} and K_i data were consistent with therapy response. The lesion-based results are shown in Table 2.

Table 1. Comparison of tumour parameters at baseline and at follow-up after hormonal therapy. K_i units are mL/min/m.

Patient/Met. no.	Baseline			Follow-up (3-6 months)			% Change		
	K_i	SUV_{mean}	SUV_{max}	K_i	SUV_{mean}	SUV_{max}	K_i	SUV_{mean}	SUV_{max}
1/1	0.12	15	22.38	0.1	14.58	21.75	-19	-3	-3
1/2	0.19	18.2	28.49	0.18	14.93	22.98	-7	-18	-19
1/3	0.29	35.9	57.92	0.14	26.27	40.45	-50	-27	-29
1/4	0.07	11.66	16.45	0.06	8.29	12.14	-24	-29	-26
1/5	0.05	10.31	14.43	0.05	6.52	9.54	-6	-37	-34
2/1	0.55	48.58	69.36	0.36	35.26	50.57	-34	-27	-27
2/2	0.58	47.84	67.37	0.22	21.14	33.2	-63	-56	-51
2/3	0.72	59.61	85.4	0.2	24.01	37.08	-72	-60	-57
2/4	0.22	19.63	29.76	0.11	18.3	26.22	-51	-7	-12
2/5	0.2	22.15	23.99	0.22	20.87	30.07	8	-6	25
2/6	0.3	29.09	42.52	0.1	7.67	11.63	-68	-74	-73
2/7	0.23	23.59	37.49	0.15	16.18	22.97	-37	-31	-39
3/1	0.35	36.01	56.56	0.18	20.88	30.07	-49	-42	-47
3/2	0.29	26.09	39.99	0.17	22.01	29.89	-41	-16	-25
3/3	0.15	17.42	23.1	0.03	13.26	18.71	-78	-24	-19
3/4	0.11	14.24	19.26	0.07	9.59	12.91	-42	-33	-33
3/5	0.16	16.82	23.97	0.12	18.08	21.89	-24	7.49	-9
							P=0.00034	P= 0.0016	P= 0.005
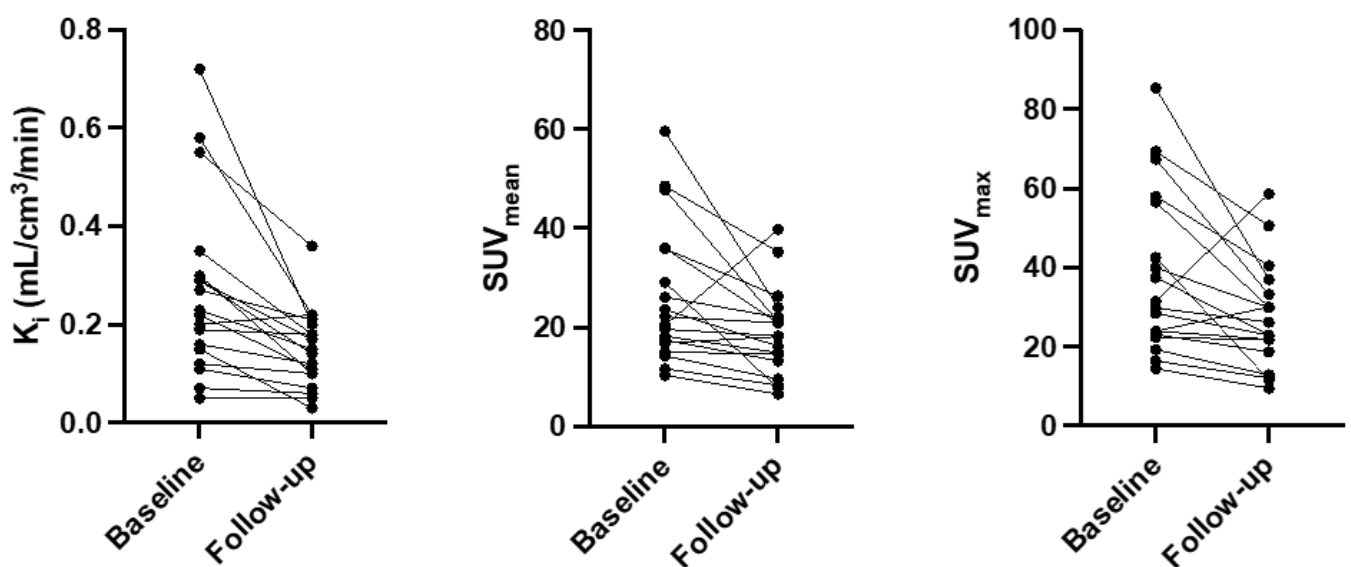
Figure 1. PET parameters at baseline and follow-up.
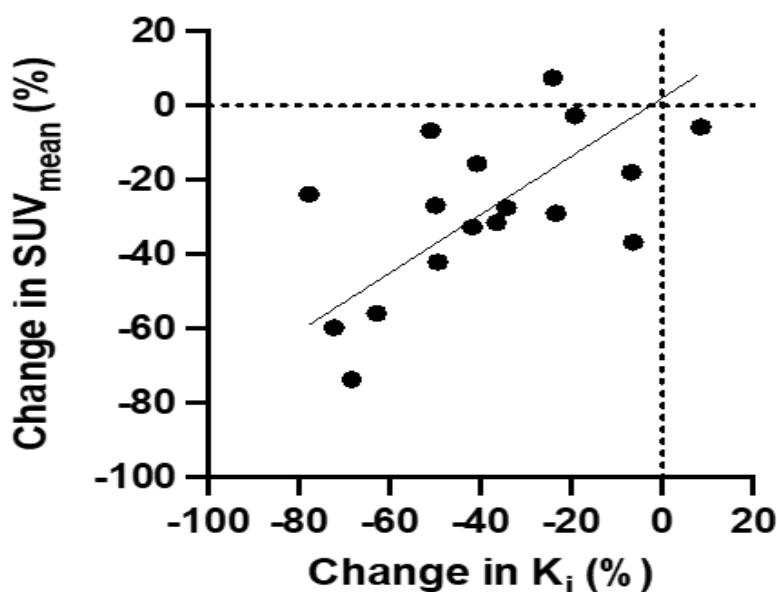
Figure 2. Relationship between changes in K_i and changes in SUV_{mean}.

Table 2. Comparison of ADC before and after treatment and assessment of changes. ADC units are mm^2/s.

Patient/Met no.	Baseline ADC	Follow-up ADC	Mean change in ADC	% Change
1/1	1085	1321	237	22
1/2	1111	969	-143	-13
1/3	1362	1517	156	11
1/4	789	1379	591	75
1/5	1499	1809	309	21
2/1	1272	1279	7	1
2/2	1158	1077	-81	-7
2/3	1442	1277	-165	-11
2/4	1031	1054	23	2
2/5	1214	1157	-57	-5
2/6	1261	1538	277	22
2/7	1569	1649	80	5
3/1	1060	1220	161	15
3/2	838	790	-48	-6
3/3	572	1016	444	78
3/4	1197	812	-385	-32
3/5	914	1319	405	44
			P=0.081	

PDFF

In the patient-based analysis, the percentage change in PDFF increased, ranging from 14% to 85%. The baseline median PDFF measurement was 16% and at follow-up median PDFF value was 17%. The median change in PDFF at follow-up was 0.7 percentage points (9%), which was consistent with conversion to a fattier marrow (P=0.229). In the lesion-based analysis, 11/17 metastases showed increased PDFF at follow-up. Remaining 6 metastases showed decreased PDFF post-therapy. The lesion-based results are shown in Table 3.

R_2^* $(1/T_2^*)$

In the lesion-based analysis, the median R_2^* at baseline was 115 s^{-1}, which increased to 126 s^{-1} at follow-up. There was a median increase of 11 s^{-1} in R_2^* after treatment, corresponding to 12%, possibly due to new bone formation and micro-calcification (P=0.001). Stable or increased R_2^* measurements were seen in 15/17 metastases and only 2 metastases showed decreasing values. The lesion based data is shown in Table 4. Overall increasing R_2^* was seen on a per-patient basis, ranging from 9.6% to 56.6%.

Table 3. Comparison of PDFF before and after treatment and assessment of changes.

Patient/Met.no.	Baseline PDFF	Follow-up PDFF	Mean change in PDFF	% Change PDFF
1/1	14.78	16.77	1.99	13
1/2	6.51	7.22	0.71	11
1/3	9.92	10.03	0.11	1
1/4	16.44	26.99	10.54	64
1/5	26.33	21.77	-4.55	-17
2/1	3.05	10.92	7.87	258
2/2	6.27	-0.03	-6.31	-101
2/3	2.72	14.93	12.22	450
2/4	9.01	9.09	0.08	1
2/5	20.32	22.21	1.9	9
2/6	10.78	9.28	-1.5	-14
2/7	20	18.35	-1.65	-8
3/1	20.07	44.31	24.24	121
3/2	16.94	19.57	2.62	15
3/3	16.39	13.32	-3.07	-19
3/4	26.3	28.68	2.38	9
3/5	29.4	23.23	-6.17	-21
			P=0.229	

Table 4. Comparison of R_2^* before and after treatment and assessment of changes. R_2^* units are s^{-1}.

Patient/Met. no.	Baseline R_2^*	Follow-up R_2^*	Mean change in R_2^*	% Change R_2^*
1/1	71.9	83.7	11.8	16
1/2	151.05	169.1	18.05	12
1/3	101.65	113.43	11.78	12
1/4	125.01	125.65	0.64	1
1/5	197.75	213.03	15.27	8
2/1	118.61	122.72	4.11	3
2/2	67.42	225.36	157.94	234
2/3	85.1	124.51	39.41	46
2/4	148.28	159.64	11.36	8
2/5	123.26	156.35	33.08	27
2/6	104.38	142.85	38.47	37
2/7	114.74	161.79	47.04	41
3/1	126.66	94.28	-32.38	-26
3/2	112.17	125.54	13.38	12
3/3	128.37	120.34	-8.03	-6
3/4	91.58	98.05	6.47	7
3/5	82.98	136.18	53.2	64
			P=0.001	
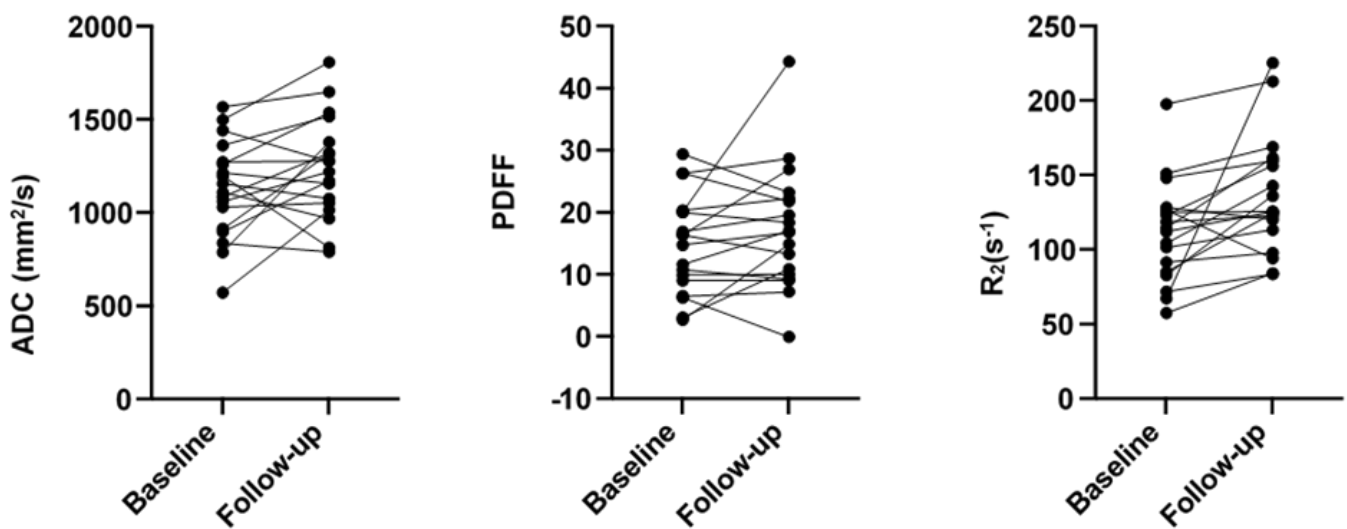
Figure 3. MRI parameters at baseline and follow-up.

There were no correlations between K_i, SUV_{max}, SUV_{mean} versus the three MRI parameters, ADC, PDFF and R* shown in Figure 3.

Discussion

In this study, [18F]NaF-PET/MRI was found feasible for monitoring hormonal therapy response in breast cancer bone metastases, as reflected by the significant SUV and K_i decreases, and the changes in MRI parameters consistent with the response. In current standard of care, monitoring of MBC treatment response mainly relies on tumour size measurements on CT/MRI according to RECIST 1.1. However, this is restricted to solid soft tissue lesions and bone metastases may only be assessed qualitatively as non-target lesions and are consistently difficult to evaluate for response. Increasing lesion density on CT, because of sclerosis, constitutes a sign of therapy response, but bone metastases frequently escape detection on baseline CT, and the appearance of sclerotic bone metastases on follow-up CT may therefore be misinterpreted as appearance of new lesions and progressive disease.

[18F]Fluoro-deoxy-glucose (FDG)-PET/CT constitutes another means for assessment of therapy response that also includes bone metastases [10]. Quantification on FDG-PET utilizes several PET biomarkers, such as the tumour SUV, metabolic tumour volume and total lesion glycolysis, which are parameters for therapy monitoring of various cancers including breast cancer [8]. In breast cancer patients, SUV changes on FDG-PET/CT have been applied for assessment of therapy response [11]. SUV measurements are easy to perform, robust, reproducible and are therefore widely used. However, true quantitative assessment of a particular tracer is not possible on static PET examinations [12]. The rate at which the tracer changes its concentration in the tissues throughout the PET examination may instead be quantified by means of a dynamic acquisition [13]. Time activity curves are derived, representing kinetic data of the tissues, and by kinetic modeling different models may be tested for the best fit to the data, and the various transport rate constants for that model can be calculated. Further, parametric images may be generated.

Doot et al. previously applied kinetic analysis on [18F]NaF-PET in MBC patients with bone metastases and showed that the fluoride transport and K_i provided a robust method to assess therapy response in bone metastases [14]. In the present study, [18F]NaF-PET/MRI was utilized to quantify the K_i, SUV_{max} and SUV_{mean} along with MRI quantitative parameters to assess hormonal therapy response in skeletal metastases. In contrast to SUV, routinely measured on static whole-body PET, quantification of [18F]NaF-influx rate K_i requires dynamic PET acquisition, which is not part of clinical routine because of the additional time requirements and the need to be started simultaneously with the tracer injection and continued for about 45 minutes. Together with the subsequent whole-body examination, every patient therefore needs to occupy the PET/CT scanner for a longer time. The introduction of new multidetector ring systems, allowing for fast simultaneous PET acquisition of the whole body, may however permit dynamic examinations of some patients with maintained throughput. Dynamic PET imaging of bone with the use of [18F]NaF is therefore a very attractive technique, as it gives an insight into the physiologic basis of "bone tracer kinetics". The bony trabeculae account for 80% of the surface area of bones and hence, of the bone turn-over. The diffusion of [18F]NaF from the capillaries into the bone extracellular fluid provides an evidence of the chemisorption of fluoride crystals at the new mineralization sites on the bone. The fluoride ions are exchanged with hydroxyl ions in the hydroxyapatite crystals and form stable fluoro-apatite present in healthy bone [15]. In previous studies, testing several models to assess fluoride kinetics, a compartment model applying non-linear regression, was found the most accurate for this quantification [16]. In our study, fluoride kinetics was assessed by two-tissue compartment model with non-linear regression to quantify the four kinetic parameters K_1-k_4 and their changes correlated with those of SUV_{mean}, and SUV_{max} [17]. The decreases in SUV_{mean}, SUV_{max} and K_i were found consistent with response to hormonal therapy and in line with the patients' clinical response. As expected, the changes in K_i, i.e. from baseline to follow-up, correlated with those of SUV_{max} and SUV_{mean}. Despite of the fact that we investigated merely three patients, lesion-based statistical analyses were possible due to the large number of bone metastases. In the lesion-based analysis, the changes in K_i, SUV_{max} and SUV_{mean} were also consistent with therapy response, except for one metastasis.

To the best of our knowledge, previously for therapy monitoring, the diagnostic accuracy of PDFF and R_2*, derived from Dixon MRI and ADC derived from DWI have not been studied in bony metastases in breast cancer patients. DWI with ADC mapping improves MRI evaluation of treatment response by providing quantitative functional assessment of cellularity, and can especially be important when intravenous contrast-enhancement is not possible. DWI is currently incorporated in many MRI routine protocols and has for some applications substituted contrast-enhanced MRI [18]. Bolan et al., studied 9 women with gynecological cancers to assess the effect of hormonal therapy on the bone marrow using Dixon MRI. An increased PDFF in the vertebral bone marrow (p=0.04) and in the femoral neck (p=0.03)

has previously been observed after 6 months of therapy compared to pre-treatment [19]. The combined information from bone marrow PDFF and multi-peak fat corrected R_2^* may even offer improved diagnostic accuracy in detection of skeletal changes such as in osteoporosis [20].

We found that MRI showed changes in ADC, PDFF and R_2^*, consistent with response, although only R_2^* reached statistical significance. In the lesion-based analysis, 11/17 of the metastases showed a relative increase in ADC at follow-up, consistent with decreased cellularity in the metastases because of cell death and development of tumour necrosis. The rise in ADC occurs in parallel with increased water diffusivity in areas of necrotic tissue post-therapy suggestive of successful treatment. Conversely, in the remaining 6/17 metastases, ADC at follow-up was lower than at baseline, which is not an expected result of favourable therapy response, and therefore not as easily explained. This could be due to a return of normal fatty bone marrow in the tumour VOI, or possible because of a sclerotic reaction as a part of the osteoblastic healing mechanism may be due to denosumab. Further, because of their lower water content, the sensitivity of DWI for sclerotic bone lesions is lower, which constitutes a potential pitfall [18].

As the present DWI protocol was only based on three b-values (50, 400 and 800), for purpose of reducing the acquisition time, the Intra-Voxel Incoherent Motion (IVIM)-derived perfusion fraction and associated pseudo-diffusion were not estimated in our study. Compared to the overall tumor water content, the fraction of blood flow is very small. IVIM, includes the microscopic movement of water molecules due to both diffusion and capillary perfusion. The perfusion component is significant at small b values and can be estimated from DWI sequences acquired with a range of high and low b-values [21]. While all patients at follow-up showed an overall increase in PDFF, the lesion-based analysis showed an increase in 11/17 metastases except in 6/17 lesions, which conversely showed a decrease. In clinical practice, the use of Dixon technique for PDFF quantification can potentially cause misinterpretation when in-phase and opposed-phase images are visually compared, since lesions consisting of pure fat exhibit no or little signal drop-out on opposed-phase images. Measured PDFF values will therefore be inaccurate or heavily influenced by fat-water ambiguity [22]. Further, a substantial spatial heterogeneity of PDFF, related to the contents of red and yellow bone marrow, is also found to exist in the different parts of the skeleton [19]. This normal variation can potentially obscure treatment response assessment based on PDFF. Like PDFF, the patient-based analysis of R_2^* data were consistent with therapy response. Lesion-based analysis for 15/17 metastases showed an increase of R_2^*, reflecting an osteoblastic reaction in the metastases, as new bone formation takes place, which increases the microscopic susceptibility effects [20].

Conclusion

In conclusion [18F]NaF PET/MRI proved feasible for monitoring of hormonal therapy response in breast cancer bone metastases, as reflected by the parallel significant decreases in SUV and K_i, and of the changes in the MRI parameters ADC, PDFF and R_2^*, consistent with the response although only R_2^* reached statistical significance. This warrants further assessment in a larger patient population.

References

1. Glendenning, Jennifer and Cook Gray. "Imaging Breast Cancer Bone Metastases: Current Status and Future Directions." *Semin Nucl Med* 43(2013): 317-323.

2. Solomayer, Erich-Franz, Diel Ingo Jakob, Meyberg Gabriele and Christian Gollan, et al. "Metastatic Breast Cancer: Clinical Course, Prognosis and Therapy Related to the First Site of Metastasis." *Breast Cancer Research and Treatment* 59(2000): 271-278.

3. Dittrich, Christian, Michael Kosty, Svetlana Jezdic and Doug Pyle, et al. "ESMO/ASCO Recommendations for a Global Curriculum in Medical Oncology Edition 2016." *ESMO Open* 1(2016): 5.

4. O'Sullivan, Gerard, Fiona L Carty and Carmel G Cronin. "Imaging of Bone Metastasis: An Update." *World J Radiol* 7(2015):202.

5. Li, Shuo, Fei Sun, Zheng-yu Jin and Hua-Dan Xue et al. "Whole-Body Diffusion-Weighted Imaging: Technical Improvement and Preliminary Results." *J Magn Reson Imaging* 26(2007):1139-1144.

6. K'Woolf, David, Padhani R Anwar and Makris Andreas. "Assessing Response to Treatment of Bone Metastases from Breast Cancer: What Should be the Standard of Care?" *Ann Oncol* 26(2015):1048-1057.

7. Tateishi, Ukihide, Cristina Gamez, Dawood Shaheenah, and Henry WD Yeung, et al. "Bone Metastases in Patients with Metastatic Breast Cancer: Morphologic and Metabolic Monitoring of Response to Systemic Therapy with Integrated PET/CT." *Radiology* 247(2008):189-196.

8. K'Azad, Gurdip, Francois Cousin, Musib Siddique and Benjamin Taylor, et al. "Does Measurement of First-Order and Heterogeneity Parameters improve Response Assessment of Bone Metastases in Breast Cancer Compared to Suv_{max} in [18F]Fluoride and [18F]FDG PET?." *Mol Imaging Biol* 21(2019):781-789.

9. Messiou, Christina and Nanditha M desouza. "Diffusion Weighted Magnetic Resonance Imaging of Metastatic Bone Disease: a Biomarker for Treatment Response Monitoring." *Cancer Biomarkers* 6(2009):21-32.

10. K'Azad, Gurdip, Musib Siddique, Benjamin Taylor and Adrian Green, et al. "Is Response Assessment of Breast Cancer Bone Metastases Better with Measurement of 18F-Fluoride Metabolic Flux than with Measurement of 18F-Fluoride PET/CT SUV?" *J Nucl Med* 60(2019)322-327.

11. Humbert, Oliver, Alexandre Cochet, Bruno Coudert and Alina Berriolo-Riedinger, et al. "Role of Positron Emission Tomography for the Monitoring of Response to Therapy in Breast Cancer." *Oncologist* 20(2015):94-104.

12. Bindoli, Sara, Paola Galozzi, Fabio Magnani and Cristina Campi, et al. "8F-Fluorodeoxyglucose Positron Emission Tomography and Computed Tomography With Magnetic Resonance for Diagnosing Adult-Onset Still's Disease." *Front Med* 7(2020):544412.

13. Rahmim, Arman, Martin Lodge, Nicolas Karakatsanis and Vladimir Y Panin, et al. "Dynamic Whole-Body PET Imaging: Principles, Potentials and Applications." *Eur J Nucl Med Mol Imaging* 46(2019):501-518.

14. K'Doot, Robert, Mark Muzi, Lanell Peterson and Erin Schubert, et al. "Kinetic Analysis of 18F-Fluoride Pet Images Of Breast Cancer Bone Metastases." *J Nucl Med* 51(2010):521-527.

15. M'Blake, Glen, So-Jin Park-Holohan, Gary JR Cook and Ignac Fogelman. "Quantitative Studies of Bone with the use of 18F-Fluoride and 99mtc-Methylene Diphosphonate." *Semin Nucl Med* 31(2001):28-49.

16. Raijmakers, Pieter, Olivier Temmerman, Carrol P Saridin and Ide C Heyligers, et al. "Quantification of 18F-Fluoride Kinetics: Evaluation of Simplified Methods." *J Nucl Med* 55(2014):1122-1127.

17. A'Hawkins, Randall, Yong Choi, Sung-Cheng Huang and Carl K Hoh, et al "Evaluation of the Skeletal Kinetics of Fluorine-18-Fluoride Ion with PET." *J Nucl Med* 5(1992):633-642.

18. Ty, Subhawong, Michael Jacobs and Laura M Fayad. "Diffusion-Weighted MR Imaging for Characterizing Musculoskeletal Lesions," *Radiographics* 34(2014):1163-1177.

19. J'Bolan, Patrick, Luke Arentsen, Thanasak Sueblinvong and Yan Zhang, et al. "Water-Fat MRI for Assessing Changes in Bone Marrow Composition due to Radiation and Chemotherapy in Gynecologic Cancer Patients." *J Magn Reson Imaging* 38(2013):1578-1584.

20. Kühn, Jens-Peter, Deigo Hernando, Peter J Meffert and Scott Reeder, et al. "Proton-Density Fat Fraction and Simultaneous R_2^* Estimation as an MRI Tool for Assessment of Osteoporosis." *Eur Radiol* 23(2013):3432-3439.

21. Denis Le Bihan. "What can we see with IVIM MRI?" *Neuroimage* 187(2019):56-67.

22. Bray, Timophy, Manil D Chouhan, Shonit Punwani and Alan Bainbridge, et al. "Fat Fraction Mapping using Magnetic Resonance Imaging: Insight into Pathophysiology." *Br J Radiol* 91(2018):20170344.